

X-MethaneWet: A Cross-scale Global Wetland Methane Emission Benchmark Dataset for Advancing Science Discovery with AI

Yiming Sun
University of Pittsburgh
Pittsburgh, PA, USA
yimingsun@pitt.edu

Shuo Chen
Purdue University
West Lafayette, IN, USA
chen4371@purdue.edu

Shengyu Chen
University of Pittsburgh
Pittsburgh, PA, USA
SHC160@pitt.edu

Chonghao Qiu
University of Pittsburgh
Pittsburgh, PA, USA
CHQ29@pitt.edu

Licheng Liu
University of Minnesota
Minneapolis, MN, USA
lichengl@umn.edu

Youni Oh
NOAA Global Monitoring Laboratory
Boulder, CO, USA
youmi.oh@noaa.gov

Sparkle L. Malone
Yale University
New Haven, CT, USA
sparkle.malone@yale.edu

Gavin McNicol
University of Illinois Chicago
Chicago, IL, USA
gmcnicol@uic.edu

Qianlai Zhuang
Purdue University
West Lafayette, IN, USA
qzhuang@purdue.edu

Chris Smith
NOAA Global Monitoring Laboratory
Boulder, CO, USA
chris.c.smith@noaa.gov

Yiqun Xie
University of Maryland
College Park, MD, USA
xie@umd.edu

Xiaowei Jia
University of Pittsburgh
Pittsburgh, PA, USA
xiaowei@pitt.edu

Abstract

Methane (CH_4) is the second most powerful greenhouse gas after carbon dioxide and plays a crucial role in climate change due to its high global warming potential. Accurately modeling CH_4 fluxes across the globe and at fine temporal scales is essential for understanding its spatial and temporal variability and developing effective mitigation strategies. In this work, we introduce the first-of-its-kind cross-scale global wetland methane benchmark dataset (X-MethaneWet), which synthesizes physics-based model simulation data from TEM-MDM and the real-world observation data from FLUXNET- CH_4 . This dataset can offer opportunities for improving global wetland CH_4 modeling and science discovery with new AI algorithms. To set up AI model baselines for methane flux prediction, we evaluate the performance of various sequential deep learning models on X-MethaneWet. Furthermore, we explore four different transfer learning techniques to leverage simulated data from TEM-MDM to improve the generalization of deep learning models on real-world FLUXNET- CH_4 observations. Our extensive experiments demonstrate the effectiveness of these approaches, highlighting their potential for advancing methane emission modeling and identifying new opportunities for developing more accurate and scalable AI-driven climate models.

Permission to make digital or hard copies of all or part of this work for personal or classroom use is granted without fee provided that copies are not made or distributed for profit or commercial advantage and that copies bear this notice and the full citation on the first page. Copyrights for components of this work owned by others than the author(s) must be honored. Abstracting with credit is permitted. To copy otherwise, or republish, to post on servers or to redistribute to lists, requires prior specific permission and/or a fee. Request permissions from permissions@acm.org.

KDD '26, Jeju Island, Republic of Korea

© 2026 Copyright held by the owner/author(s). Publication rights licensed to ACM.
ACM ISBN 979-8-4007-2258-5/2026/08
<https://doi.org/10.1145/3770854.3785682>

CCS Concepts

• **Applied computing** → **Environmental sciences**; • **Computing methodologies** → **Machine learning**; • **Information systems** → **Data mining**; **Spatial-temporal systems**.

Keywords

Methane Emission, Transfer Learning, AI for Science, Spatial-temporal Modeling, Knowledge-guided Machine Learning

1 Introduction

Methane (CH_4) is the second most important greenhouse gas after carbon dioxide [59]. CH_4 has significant implications for climate change due to its high global warming potential [3, 47]. Wetlands, as the largest natural source of CH_4 , emitted 159 [119-203] Tg CH_4 yr⁻¹ globally during 2010-2019 [55] and accounted for nearly one-third of total global CH_4 emissions[21]. Accurately modeling wetland CH_4 fluxes on a fine temporal scale is critical for understanding its spatial and temporal dynamics and informing mitigation strategies. Due to its relatively short atmospheric lifetime and greater per-molecule radiative forcing compared to other greenhouse gases, reduction of methane is often considered an effective way of mitigating climate change. However, the modeling of methane emission is very challenging as methane emissions are highly variable in space and time, influenced by hydrological conditions, temperature, and microbial activities.

Over the past decades, physics-based (PB) models have traditionally been used for the estimate of wetland CH_4 emissions. PB models use mathematical equations to explain the connection between the CH_4 production, oxidation, and transport processes and environmental variables [61, 72]. For example, the Terrestrial Ecosystem Model with Methane Dynamics Module (TEM-MDM) simulates

methanogenesis in the saturated zones of soil and methanotrophy in the unsaturated zones, with both processes influenced by soil temperature, moisture, and organic carbon availability [75]. TEM-MDM also simulates methane transport through soil layers by diffusion, plant-aided transport, and ebullition, allowing for a dynamic representation of how methane moves from the soil to the atmosphere, particularly in wetland areas [75]. By incorporating mechanistic relationships and physical laws, PB models can predict system responses to various scenarios, including those outside the range of historical observations [36]. However, PB models require extensive parametrization and complex calculations, which can limit their applicability in real-time or large-scale scenarios.

More recently, there is a growing interest in using ML methods for estimating wetland CH₄ emission [8, 15, 20, 26, 27, 44, 51, 70]. Compared to traditional PB models, ML models are much more computationally efficient during inference while also effectively capturing complex nonlinear patterns in CH₄ flux data. However, due to the absence of large training datasets, traditional ML approaches may lack generalizability to out-of-sample prediction scenarios, e.g., testing in different regions or performing future time projections. This is further exacerbated by the spatial and temporal variability in wetland methane observations. Hence, a comprehensive benchmark dataset is urgently needed for the development of robust ML-based models.

One ML-based research direction involves employing ML models to upscale eddy covariance (EC) measurements into global wall-to-wall flux maps [8, 44, 51, 70]. These ML models rely on globally available predictors such as meteorological data and soil properties to build empirical models at the site level before estimating CH₄ fluxes across all wetland grid cells. The upscaling products could serve as benchmark datasets but also come with inherent uncertainties, such as the choice of ML models, predictor variables, and forcing data. Despite their potential as benchmark datasets, the CH₄ modeling community still lacks a systematic benchmarking framework that offers standardized models, evaluation metrics, and datasets for rigorously comparing and assessing future work.

In this work, we introduce X-MethaneWet, the first global wetland methane dataset that integrates physical simulations generated by TEM-MDM and true observations at a daily scale. The TEM-MDM-based simulated dataset contains the simulation of CH₄ fluxes across 62,470 global sites, providing a comprehensive dataset for evaluating model performance under controlled conditions. The FLUXNET-CH₄ dataset, on the other hand, consists of observed CH₄ fluxes from 30 wetland sites worldwide, representing real-world conditions with varying environmental factors. Such an integrative dataset enables the evaluation of ML models in both emulating PB models and predicting actual methane fluxes over large spatial scales and long time periods. More importantly, we establish a standardized evaluation framework to assess the generalizability of methane prediction model across space and time. Such an evaluation framework defines specific spatial and temporal generalization test cases, along with the evaluation metrics that best fit the task of methane prediction.

Based on the established evaluation framework, we conduct comprehensive experiments using a range of ML models, which include LSTM-based models (e.g., LSTM [18] and EA-LSTM [34]), the temporal CNN-based model [33], and Transformer-based models (e.g.,

Transformer [66], iTransformer [39], and Pyraformer [37]). These tests demonstrate the promise of existing ML models in capturing complex CH₄ emission dynamics at the fine temporal frequency (daily scale) from input drivers and predicting CH₄ emissions for unobserved regions and future time periods. The comparison among these models also allows for analyzing the gap and opportunities of current ML models in the context of methane prediction.

In addition to the standard ML benchmark testing, our integrative dataset also enables the exploration of knowledge transfer approaches from TEM-MDM-based simulated data to facilitate capturing observed CH₄ flux dynamics. This is inspired by recent advances in knowledge-guided machine learning (KGML) [24, 25, 68], which aims to leverage the complementary strengths of both PB and ML models. Previous work in this field has shown that pre-training an ML model with simulated data generated by PB models can facilitate learning general physical patterns. Then this pre-trained model needs only a few observations to correct the simulation bias during fine-tuning to achieve a quality model [23, 52, 53]. In addition to this pretrain-finetune approach, we have also applied multiple transfer learning algorithms to all previously considered ML models to test their performance with knowledge adapted from physical simulations. This experiment demonstrates the effectiveness of knowledge transfer in improving the generalization capabilities of ML models, especially in data-sparse scenarios. The results highlight the potential of integrating synthetic data with real-world observations to develop more accurate, robust, and scalable AI-driven models for wetland CH₄ flux estimation, contributing to better climate modeling and mitigation strategies.

Our dataset and implementation of benchmark testing have been released¹. Our contributions have been summarized as follows:

- We create the first integrative global wetland CH₄ dataset that combines both physical simulations and true observations. Additionally, it is the first CH₄ dataset to provide global-scale methane simulations at daily resolution.
- We introduce a standardized evaluation framework for testing ML models in global high-frequent methane flux prediction. This is particularly designed with test cases and evaluation metrics to validate model generalizability over space and time.
- We conduct comprehensive tests of diverse ML models and analyze their performance in both emulating the physics-based TEM-MDM model and predicting truly observed methane emissions. We further apply multiple transfer learning approaches on these ML models, which shows the opportunities in leveraging knowledge from TEM-MDM-generated physical simulations to facilitate the prediction in data-sparse scenarios.

2 Related Work

2.1 CH₄ benchmark data

Recently, significant efforts have been dedicated to developing benchmark data for CH₄ emissions. Most of these works utilize simple models to upscale CH₄ measurements to larger regions and higher resolution. A random forest (RF) model has been utilized to upscale CH₄ eddy covariance flux measurements from 25 sites for the northern region [51]. Also, a causality-guided long short-term

¹<https://huggingface.co/datasets/ymsun99/X-MethaneWet> (Dataset) and <https://github.com/ymsun99/X-MethaneWet> (Code)

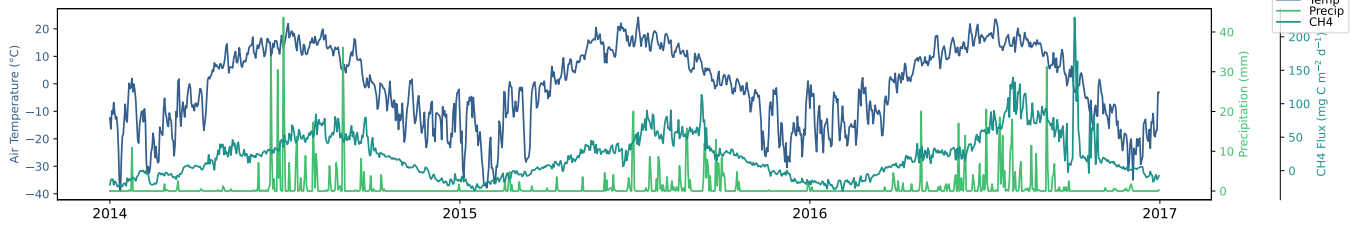


Figure 1: Temporal variations in air temperature, precipitation, and CH₄ flux across 2014 to 2016 in US.BZB site.

memory (causal-LSTM) model was developed and utilized data from 30 eddy covariance towers across four wetland types: bog, fen, marsh, and wet tundra [70]. The causal-LSTM outperformed the traditional LSTM by integrating causal relationships derived from transfer entropy analysis into the modeling process. The upscaled product is at 0.5° spatial resolution and covers the northern boreal and arctic regions. The time period is from 2000 to 2018 at weekly temporal resolution. The aforementioned datasets primarily focus on the Northern boreal and arctic regions. The first global benchmark dataset (UpCH₄) was produced using an RF model that trained from 45 FLUXNET-CH₄ sites [44]. UpCH₄ is at 0.25° spatial resolution and global spatial coverage. The time period is from 2000 to 2018 at monthly temporal resolution. Later, another global CH₄ benchmark data was produced by multi-model ensemble mean of six ML models, including decision tree, RF, XGB, ANN, Gated Recurrent Units, and LSTM [8]. This dataset was upscaled from 82 eddy covariance and chamber sites. It is at 0.5° spatial resolution and global spatial coverage. The time period is from 2000 to 2020 at monthly temporal resolution. Though great efforts were made to develop global methane benchmark datasets, no existing work has produced datasets at a daily resolution, nor clearly outlined the benchmarking protocols, prohibiting the broad implementation of those datasets, especially for AI model development. Different from these datasets, we provide the first integrative dataset that consists of both simulated data and true observation data. The simulations are at high spatial resolution, and true observation data are from multiple sites worldwide at the daily scale. Meanwhile, we provide a standardized evaluation framework to accelerate future AI model development for estimating methane emission.

2.2 Machine learning for CH₄ prediction

Multiple ML models for estimating CH₄ emissions have been developed and tested in existing research. The artificial neural networks (ANNs) was utilized in the early research to predict CH₄ emissions in drained and flooded agricultural peatlands in the Sacramento-San Joaquin Delta [15]. The ANN model was also utilized to predict CH₄ emissions across 60 FLUXNET-CH₄ sites [27]. Furthermore, the performance of multiple ML models, including ANNs, random forests (RF), and support vector machines (SVM) [26] were compared in the later research. RF model was found to outperform the other models across various test scenarios and sites. Another research compared the performance of Lasso regression (Lasso), ANNs, RF, and extreme gradient boosting (XGBoost). RF also outperformed the other ML models in terms of normalized mean absolute error (nMAE) and coefficient of determination (R^2) across 17 FLUXNET-CH₄ sites [20]. However, the ML models tested in the previous research primarily focus on gap-filling rather than benchmarking.

Many other deep learning models have shown encouraging results in ecological modeling and thus can also be considered promising candidates for methane emission prediction. For example, long short-term memory and its variants, such as EA-LSTM [30], incorporate gating mechanisms to capture long-term dependencies in sequential data. They are reported to outperform many advanced models in simulating ecosystem dynamics [35, 69]. Temporal convolution networks (TCN) [33] leverage causal and dilated convolutions to model long-range dependencies, and have also been used in many environmental applications [50, 60, 62]. Transformer-based models, such as the vanilla Transformer [13, 66], iTransformer [39], and Pyraformer [37], use self-attention mechanism and have gained attention in many long-term forecasting tasks such as predicting weather and climate changes, as well as energy potential. Despite the promise of advanced ML models, they often lack generalizability to data-sparse scenarios. Recent advances in knowledge-guided machine learning (KGML) [24, 25, 68] address this issue by leveraging accumulated scientific knowledge to guide the learning process of ML models. Prior work in KGML has shown that the pretraining ML models on PB simulated data can help significantly enhance the predictive performance in monitoring poorly-observed ecosystems [23, 52, 53]. However, similar approaches have yet been developed for estimating wetland CH₄ emissions.

3 Dataset Construction

The X-MethaneWet dataset integrates both simulated and observed CH₄ data from different sources and different scales. In the following, we describe how we create the simulated data using the TEM-MDM model and the observation data from FLUXNET-CH₄.

3.1 Simulated data: TEM-MDM

TEM-MDM enhances existing PB models by explicitly accounting for permafrost freeze-thaw dynamics and vegetation carbon dynamics, as well as simulating methane production, oxidation, and transport processes on an hourly basis [75]. We conduct global CH₄ flux intensity simulations using TEM-MDM at a daily and 0.5-degree resolution from 1979 to 2018. The drivers include ERA-Interim climate data [9], vegetation type (c1tveg) [45], plant function type (vegetation_type_11) [43], topsoil bulk density (topsoil_bulk_density) [46], sand, silt, and clay fractions (c1faatxt) [74], pH (pH2o) [6], wetland types [42], elevation (clelev) [63], global annual CO₂ concentration (kco2), global annual CH₄ concentration (ch4).

Specifically, the feature set includes static, yearly, monthly and daily features, all aligned at the daily level. The climate data are at daily resolution and provide variables such as precipitation (PREC),

air temperature (TAIR), solar radiance (SOLR), and vapor pressure (VAPR) [9]. The intermittent variable net primary productivity (NPP) was generated from TEM-MDM and is on a monthly scale. We also use yearly features such as global annual CO₂ and CH₄ concentration. Categorical features, including the wetland distribution map and the spatial distribution of characteristics (e.g., vegetation) are static over time. All these features are duplicated and expanded to daily resolution. Detailed descriptions of the above features are provided in Appendix A.

Our TEM-MDM dataset consists of 62,470 spatial positions, which are continent locations filtered from the 360 × 720 grid spanning latitudes [-90°,90°] and longitudes [-180°,180°]. Each position contains daily data over a span of 40 years. We cut the original data into yearly sequences each consisting of 365 days. For the input, we use a 15-dimensional feature space, including the previously mentioned variables. More formally, after our processing, the dimensionality and total volume of input drivers is given by $N_{\text{input}} = N_S \times N_T \times N_L \times N_D$, where the spatial scale N_S , the temporal scale N_T , the sequence length N_L , and the feature dimension N_D are 62470, 40, 365, and 15, respectively. For the output, we have a single target variable for CH₄ emission. Hence, the dimensionality of our target CH₄ flux is $N_{\text{output}} = N_S \times N_T \times N_L$.

3.2 Observation data: FLUXNET-CH₄

The FLUXNET-CH₄ Version 1.0 provides standardized data on CH₄ fluxes, measured at 81 sites from multiple regional flux networks using eddy covariance (EC) technology [10]. This half-hourly and daily CH₄ fluxes data covers freshwater, coastal, upland, natural, and managed ecosystems [10]. It has been widely used for independent ground truth validation of satellite measurements and Earth system models and improving our understanding of ecosystem-scale CH₄ flux dynamics [44, 49].

We select 30 seasonal or permanent vegetated wetland sites covering bog (5), fen (7), marsh (6), swamp (2), salt marsh (3), drained (1) and wet tundra (6) wetland classes and distributed across Arctic-boreal (13), temperate (13), and (sub)tropical (4) climate zones. As shown in Figure 8, the sites used in this paper include BW-Gum [16], US-DPW [17], US-LA1 [31], US-LA2 [32], US-NC4 [48], US-Myb [41], US-Srr [2], US-ORv [4], US-MRM [56], US-OWC [5], US-WPT [7], JP-BBY [64], US-Los [11], FR-LGt [22], DE-Sfn [57], DE-Zrk [54], DE-Hte [28], CA-SCB [58], FI-Sii [67], FI-Si2 [67], US-BZB [12], US-BZF [12], FI-Lom [40], US-Ivo [76], US-ICs [12], RU-Che [14], RU-Ch2 [14], US-Atq [77], US-Bes [79], and US-Beo [78]. Figure 1 shows an example of CH₄ flux variation in the FLUXNET-CH₄ dataset alongside the two most important features, air temperature and precipitation, illustrating their relationships.

For FLUXNET-CH₄ data, the time span varies across different sites but generally ranges from 2006 to 2018. The specific time period for each site is shown in Figure 2 in Appendix B. In total, the dataset contains 109 site-years of daily sequence data. The dataset included latitude, longitude, elevation, International Geosphere-Biosphere Programme (IGBP) land cover classification for every site, and temporal information including air temperature, precipitation, vapor pressure, and CH₄ emission labels. For the X-MethaneWet dataset, we select sites classified as ‘wet’ in the IGBP classification column, resulting in a total of up to 30 sites. We use the available

values in FLUXNET-CH₄ for data constructions and derive the wetland type from the WAD2M wetland distribution map [71], as shown in Figure 8 in Appendix B. For missing features, we fill in the gaps using values from the nearest grid point in TEM-MDM, ensuring that the data is padded to a 15-dimensional feature space consistent with the TEM-MDM dataset. FLUXNET-CH₄ emission approximately range from -100 to 900 mg C m⁻² d⁻¹.

4 Evaluation Framework

4.1 Experimental test cases

An effective CH₄ predictive model should generalize well to unseen scenarios. In practice, the CH₄ predictive model is often used to make predictions for future periods or in unobserved spatial regions. Hence, we perform two different prediction tasks to reflect these real-world settings: temporal extrapolation and spatial extrapolation. The objective of the temporal extrapolation task is to evaluate the ability of a model to predict methane emission for a future period. It is noteworthy that this prediction task is different from typical forecasting as the input drivers remain available for the testing period. This is to mirror the practical setting of future prediction which relies on input drivers simulated by external models (e.g., climate models). For the spatial extrapolation task, the goal is to evaluate the model’s ability to generalize to locations not present in training data. This allows us to assess its ability to predict methane emission for completely unobserved spatial regions, e.g., regions that are distant from existing CH₄ flux towers. Due to the strong spatial heterogeneity, we conduct a multi-fold cross-validation over all the spatial locations for a more comprehensive evaluation.

Figure 2 illustrates the train-test splitting strategies applied to the FLUXNET-CH₄ dataset, including temporal extrapolation (split across years) and spatial extrapolation (split across sites), used for evaluating generalization across time and space.

4.2 Evaluation metrics

The assessment of predictive performance employs two metrics: normalized root mean squared error (nRMSE) and the coefficient of determination (R² score). Specifically, nRMSE quantifies the average magnitude of prediction errors relative to the mean of the observed data \bar{y} (defined as $\text{nRMSE} = \text{RMSE}/\bar{y}$), allowing for a more meaningful comparison across different datasets. A lower nRMSE indicates better predictive accuracy. R² score evaluates how well the model can use the input drivers to explain the variance in the target CH₄ data. The R² score has a maximum value of 1, with a higher score indicating a better fit of the model to the data. Between these two metrics, nRMSE accounts for the scale of CH₄ values while R² considers the variance of CH₄ values.

4.3 Experimental design

We conduct temporal and spatial extrapolation tasks using both the TEM-MDM-based simulated dataset and the observed FLUXNET-CH₄ dataset. Specifically, we consider three testing scenarios: predicting simulated data, predicting observed data, and transfer learning. For each testing scenario, we will perform both temporal and spatial extrapolation. More details are described as follows.

Predicting simulated data: Using TEM-MDM, in temporal extrapolation experiments, we use data from 1979 to 1998, covering a

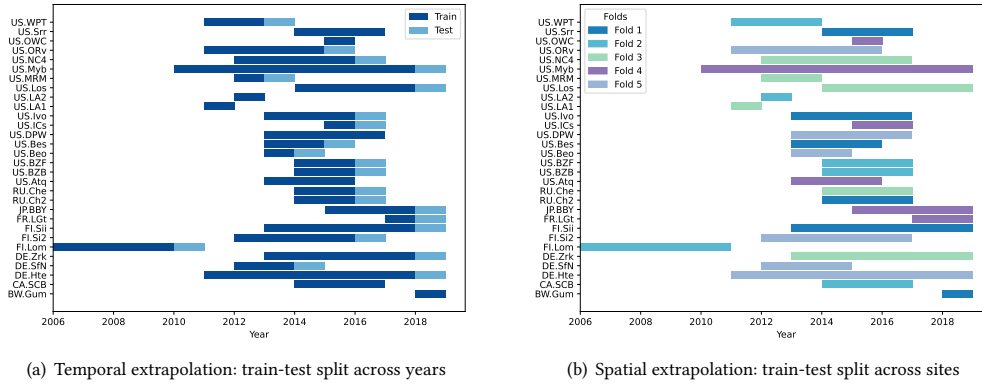


Figure 2: Train-test split of FLUXNET-CH₄ dataset for temporal and spatial extrapolation experiments.

total of 20 years for training across all locations (a total of 62,470 positions), and evaluate the models on the following period from 1999 to 2018, spanning another 20 years across all locations. For spatial extrapolation tasks, we divide all locations into five equal folds, each containing 12,494 positions. For each run, the models are trained on data from four folds, which include data from 49,976 locations over all 40 years (i.e., 1979 to 2018), and tested on the remaining fold (12,494 positions over 40 years). To ensure robustness, we perform cross-validation by rotating the test fold across different runs.

Predicting observed data: Using FLUXNET-CH₄, in temporal extrapolation experiments, we hold out the last years of certain sites for testing, while using the remaining years from all sites for training, as shown in Figure 2(a). In spatial extrapolation experiments, we divide all locations into five equal folds, each containing six sites, as shown in Figure 2(b). The models are trained using data from four folds, covering complete time periods, and tested on the remaining fold. Similar to the previous case, we perform cross-validation by rotating the test fold across different runs.

Transfer learning: Additionally, we conduct experiments to transfer knowledge from simulated data to observed data prediction. Real observations of CH₄ (e.g., the FLUXNET-CH₄ dataset) is often limited in both spatial and temporal scales, posing challenges for robust model training and generalization. To enhance performance on the FLUXNET-CH₄ dataset, we explore transfer learning methods to leverage simulated data from the TEM-MDM dataset for predicting true observations of CH₄ in the FLUXNET-CH₄ dataset. Specifically, we split the FLUXNET-CH₄ dataset in the same way as in *predicting observed data* for both temporal and spatial extrapolation tests, and use the complete TEM-MDM simulated dataset as the source domain in transfer learning.

5 Experiments

In this section, we conduct multiple experiments using a range of candidate temporal ML models to demonstrate the promise and gap in methane emission prediction.

5.1 Experimental settings

Candidate methods. We test multiple existing temporal ML models, including two traditional LSTM-based methods: LSTM [19]

and EA-LSTM [29], a temporal CNN-based model: TCN [38], and three encoder-only Transformer-based models: Transformer [66], iTransformer [39], and Pyraformer [37]. Specifically, EA-LSTM is a variant of LSTM commonly used for sequential data prediction in ecological modeling by generating the gating variables using only the static environmental characteristics (e.g., soil properties). The iTransformer and Pyraformer methods are popular methods for time-series modeling tasks, by focusing on inter-variable dependencies and multi-resolution temporal dependencies, respectively. We do not include results for the random forest model in this study, as our results indicate lower performance compared to temporal ML models in predicting daily methane emissions.

To effectively transfer information from the source domain (TEM-MDM) to the target domain (FLUXNET-CH₄), we also employ two categories of transfer learning approaches: parameter transfer and data transfer. In the parameter transfer category, models are first trained on the source domain and then utilized in the target domain. In our experiments, we implement two methods: the pre-train and fine-tune method, and the residual learning method. In the pre-train and fine-tune method, we first train the model on the TEM-MDM until convergence. We then further fine-tune the pre-trained model using the FLUXNET-CH₄. This approach allows the model to capture the inherent relationships between features and CH₄ emission in the TEM-MDM data, enabling a faster and more effective adaptation to the FLUXNET-CH₄ data. Instead of directly fine-tuning, the residual learning method leverages the pre-trained model from TEM-MDM as a baseline for the FLUXNET-CH₄. A separate model is then trained to predict the residual difference between the predicted CH₄ emission from the pre-trained model and the ground-truth CH₄ emission from FLUXNET-CH₄ data. This approach explicitly considers the discrepancies of label spaces, allowing the model to adjust the predictions based on domain-specific variations.

In the data transfer category, data from TEM-MDM is directly integrated with FLUXNET-CH₄ data to build a unified model. We implement two methods within this approach: adversarial learning and re-weighting. For adversarial learning, we adopt a method similar to Domain-Adversarial Neural Networks (DANN) [1], where a domain discriminator is trained alongside the main model to minimize the discrepancy between the TEM-MDM and FLUXNET-CH₄ data distributions. The adversarial objective encourages the

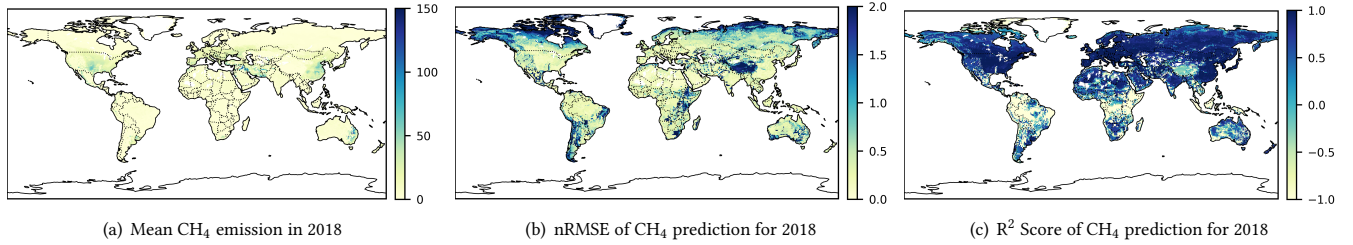


Figure 3: Label and LSTM prediction performance in the TEM-MDM dataset in 2018.

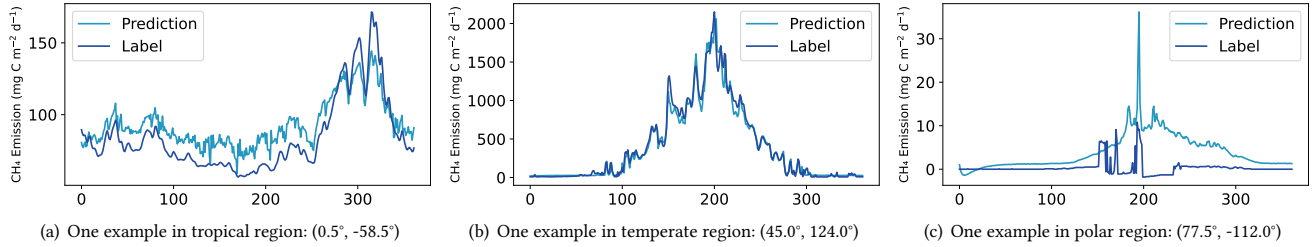


Figure 4: Comparison of LSTM predictions and labels in the TEM-MDM dataset across climate zones in 2018.

model to learn domain-invariant features, improving its generalization ability across datasets. Instead of aligning feature distributions through an adversarial objective, the re-weighting method assigns different weights to samples in TEM-MDM to better match the label distribution of FLUXNET-CH₄. The re-weighting is based on statistical properties, specifically the mean and standard deviation of the target data. We compute the differences in mean and standard deviation between TEM-MDM samples and FLUXNET-CH₄ data as a measure of similarity and use these similarity values to re-weight the loss function for each TEM-MDM sample. By dynamically adjusting these weights based on their relevance to the target domain, the model prioritizes FLUXNET-CH₄ data while still leveraging useful information from TEM-MDM.

Implementation details. We apply data standardization to both the training and testing datasets. Standardization is performed on both the TEM-MDM and FLUXNET-CH₄ datasets using the mean and standard deviation of the TEM-MDM dataset. All candidate methods are implemented using PyTorch 2.5 and run on a GTX 3080 GPU, using the ADAM optimizer, with an initial learning rate of

Table 1: Quantitative performance, measured by (nRMSE, R² score), is evaluated on the TEM-MDM dataset for temporal and spatial extrapolation tasks. The results are averaged over three independent runs. The results in bold highlight the best performance across models.

Method	Temporal	Spatial
LSTM	(0.68±0.03, 0.92±0.01)	(0.66±0.04, 0.92±0.01)
EALSTM	(0.97±0.01, 0.84±0.01)	(0.91±0.04, 0.86±0.01)
TCN	(1.19±0.04, 0.77±0.02)	(1.14±0.07, 0.78±0.03)
Transformer	(1.04±0.03, 0.83±0.01)	(0.78±0.03, 0.90±0.01)
iTransformer	(1.28±0.02, 0.74±0.01)	(1.29±0.03, 0.73±0.02)
Pyraformer	(1.05±0.02, 0.82±0.01)	(1.13±0.03, 0.80±0.01)

Table 2: Quantitative performance, measured by (nRMSE, R² score), is evaluated on the FLUXNET-CH₄ dataset for temporal and spatial extrapolation tasks. The results are averaged over three independent runs.

Method	Temporal	Spatial
LSTM	(1.02±0.03, 0.55±0.03)	(1.40±0.27, 0.09±0.17)
EA-LSTM	(1.14±0.03, 0.43±0.01)	(1.45±0.37, 0.04±0.31)
TCN	(1.24±0.03, 0.32±0.02)	(1.33±0.38, 0.18±0.29)
Transformer	(1.50±0.03, 0.03±0.05)	(1.50±0.18, -0.01±0.03)
iTransformer	(1.44±0.04, 0.07±0.02)	(1.38±0.26, 0.14±0.18)
Pyraformer	(1.02±0.03, 0.55±0.01)	(1.33±0.38, 0.19±0.27)

0.001. All models are set with 3 layers and hidden state dimensions of 8. Transformer-based models use 4 attention heads.

5.2 Predicting simulated data

Quantitative analysis. We report the average performance of three independent runs for each candidate method using the simulated TEM-MDM dataset from locations across the globe, as shown in Table 1. Several key observations emerge from the results: (1) Between the LSTM-based models, LSTM outperforms EA-LSTM in both temporal and spatial extrapolation tasks, achieving lower nRMSE and higher R² scores. This suggests that the simplified gating mechanism adopted in EA-LSTM may not fully capture the factors responsible for modulating the influence of input drivers on wetland states. (2) TCN performs poorly in terms of both nRMSE and R² scores across both tasks. This suggests that convolutional models are less suitable for sequential methane prediction, likely due to their inherent limitations in modeling long-range dependencies in methane flux dynamics and the lack of adaptive memory mechanisms for modeling complex dynamics. (3) Transformer-based models show varied performance. The standard Transformer

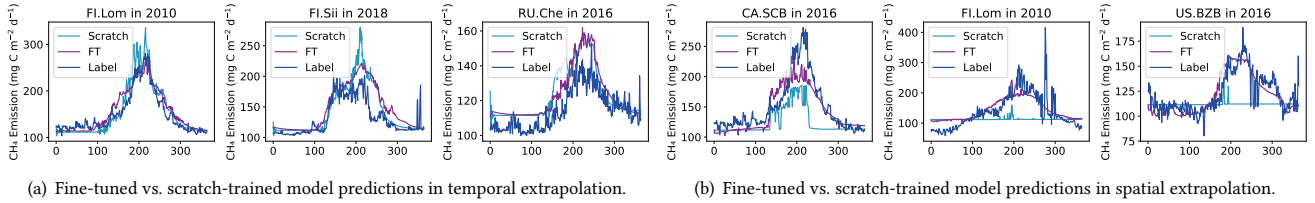


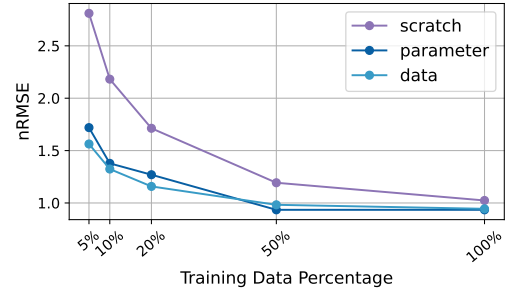
Figure 5: Examples showing performance improvements through LSTM fine-tuning in both temporal and spatial extrapolation.

model performs worse than LSTM but better than TCN. However, iTransformer and Pyraformer, which introduce specialized architectural improvements, exhibit distinct behaviors. iTransformer has the highest nRMSE and the lowest R^2 , indicating poor generalization performance. This may be due to its self-attention mechanism operating only across variables rather than across time, which limits its ability to capture methane emission dynamics. Pyraformer, on the other hand, demonstrates a more balanced performance, with an nRMSE of 1.05 in temporal extrapolation and 1.13 in spatial extrapolation, placing it between Transformer and iTransformer.

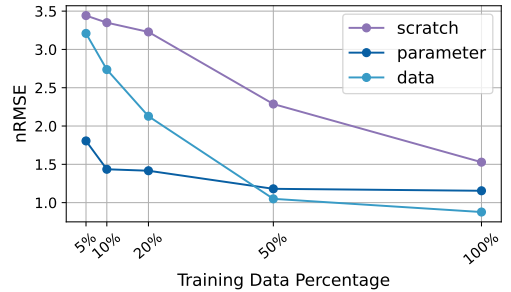
Qualitative analysis. To further analyze model performance across different positions within a single year, we evaluate an LSTM model trained on data from 1979 to 2017 and tested on 2018. Figure 3(a) presents the mean CH₄ emissions in 2018, while Figure 3(b) and Figure 3(c) show the nRMSE and R^2 score of LSTM-based CH₄ predictions for the same year. From the nRMSE and R^2 maps, we observe strong model performance in the temperate region, where both metrics indicate high accuracy. This is further illustrated in Figure 4(b), where the predictions closely align with the ground truth labels. In the tropical region, while nRMSE remains low, the R^2 score is poor. As shown in Figure 4(a), the model’s predictions tend to stay close to the target values but exhibit significant oscillations, leading to a low R^2 score. For the polar region, both nRMSE and R^2 indicate poor performance. Figure 4(c) shows that the predictions deviate noticeably from the target values, highlighting the model’s limitation in this region.

5.3 Predicting observed data

We present the average performance of each candidate method using the observed FLUXNET-CH₄ dataset from 30 sites in Table 2. It is worth noting that the standard deviation in the spatial extrapolation setting is relatively large due to the high spatial data variability across different FLUXNET-CH₄ sites. This variability significantly impacts the performance in cross-validation, leading to large fluctuations. Furthermore, since the number of observational sites is limited and spatially sparse, test sites in the spatial extrapolation setting are often far from any training sites. This makes generalization particularly difficult and may partly explain the relatively poor results, rather than indicating model overfitting. In addition, there are some observations from the results: (1) For temporal extrapolation, both LSTM and Pyraformer achieve the best results, outperforming other methods with lower nRMSE and higher R^2 . (2) The standard Transformer and iTransformer struggle in the temporal extrapolation. This suggests the limitations of these models in capturing complex methane dynamics with limited methane flux



(a) Sparsity test for LSTM



(b) Sparsity test for Transformer

Figure 6: Sparsity test results in temporal extrapolation task for LSTM and Transformer models. We compare the variants of each model with (1) learning from scratch, (2) data transfer by DANN, and (3) parameter transfer via fine-tuning.

data, which could involve both long-term and short-term temporal dependencies in practice. (3) TCN and Pyraformer both show competitive performance for spatial extrapolation. However, due to the strong spatial variability (i.e., large standard deviations), they are not consistently better than other models. (4) Compared with LSTM, EA-LSTM performs slightly worse, suggesting that its simplified gating mechanism does not necessarily enhance generalization. Overall, these observations suggest that Pyraformer remains a strong baseline for methane flux forecasting.

5.4 Transfer learning from simulations to observations

Quantitative analysis. The experimental results in Table 3 highlight the impact of transfer learning approaches on methane flux prediction based on the performance on the FLUXNET-CH₄ dataset. In particular, the “No Transfer” column represents models trained

Table 3: Detailed quantitative performance evaluation on the FLUXNET-CH₄ dataset. Each cell reports the mean and standard deviation (mean \pm std) for two metrics: the top value is nRMSE and the bottom value is R². We highlight the best transfer learning results for each model in the temporal extrapolation setting with bold and the second-best score with *italic*.

Model	No Transfer		Parameter Transfer				Data Transfer			
			Fine-tune		Residual		Adversarial		Re-weight	
	temporal	spatial	temporal	spatial	temporal	spatial	temporal	spatial	temporal	spatial
LSTM	1.02 \pm 0.03	1.40 \pm 0.27	0.93 \pm 0.07	1.30 \pm 0.42	0.96 \pm 0.06	1.33 \pm 0.35	<i>0.89 \pm 0.02</i>	1.38 \pm 0.43	0.89 \pm 0.04	1.45 \pm 0.41
	0.55 \pm 0.03	0.09 \pm 0.17	0.62 \pm 0.01	0.20 \pm 0.35	0.59 \pm 0.05	0.18 \pm 0.22	<i>0.64 \pm 0.02</i>	0.13 \pm 0.35	0.64 \pm 0.03	0.03 \pm 0.31
EA-LSTM	1.14 \pm 0.03	1.45 \pm 0.37	0.93 \pm 0.02	1.35 \pm 0.32	0.96 \pm 0.01	1.43 \pm 0.29	0.80 \pm 0.03	1.50 \pm 0.38	<i>0.86 \pm 0.02</i>	1.60 \pm 0.30
	0.43 \pm 0.01	0.04 \pm 0.31	0.60 \pm 0.01	0.15 \pm 0.22	0.59 \pm 0.01	0.04 \pm 0.18	0.71 \pm 0.02	-0.03 \pm 0.31	<i>0.67 \pm 0.02</i>	-0.16 \pm 0.59
TCN	1.24 \pm 0.03	1.33 \pm 0.38	1.12 \pm 0.02	1.40 \pm 0.36	1.15 \pm 0.03	1.30 \pm 0.29	1.05 \pm 0.09	1.50 \pm 0.29	<i>1.08 \pm 0.03</i>	1.58 \pm 0.46
	0.32 \pm 0.02	0.18 \pm 0.29	0.43 \pm 0.02	0.09 \pm 0.30	0.40 \pm 0.03	0.21 \pm 0.22	0.49 \pm 0.08	-0.06 \pm 0.25	<i>0.48 \pm 0.03</i>	-0.16 \pm 0.47
Transformer	1.50 \pm 0.03	1.50 \pm 0.18	1.15 \pm 0.01	1.40 \pm 0.42	1.12 \pm 0.03	1.40 \pm 0.33	0.86 \pm 0.01	1.40 \pm 0.29	<i>0.93 \pm 0.01</i>	1.40 \pm 0.36
	0.03 \pm 0.05	-0.01 \pm 0.03	0.42 \pm 0.01	0.09 \pm 0.33	0.43 \pm 0.01	0.10 \pm 0.18	0.66 \pm 0.01	0.08 \pm 0.34	<i>0.61 \pm 0.01</i>	0.09 \pm 0.25
iTransformer	1.44 \pm 0.04	1.38 \pm 0.26	1.05 \pm 0.03	1.43 \pm 0.39	1.44 \pm 0.07	1.48 \pm 0.35	1.18 \pm 0.02	1.38 \pm 0.41	<i>1.15 \pm 0.06</i>	1.43 \pm 0.45
	0.07 \pm 0.02	0.14 \pm 0.18	0.50 \pm 0.03	0.05 \pm 0.40	0.09 \pm 0.09	-0.01 \pm 0.30	0.38 \pm 0.02	0.13 \pm 0.33	<i>0.40 \pm 0.06</i>	0.06 \pm 0.44
Pyraformer	1.02 \pm 0.03	1.33 \pm 0.38	<i>0.86 \pm 0.04</i>	1.43 \pm 0.47	0.96 \pm 0.07	1.28 \pm 0.28	0.86 \pm 0.01	1.35 \pm 0.42	<i>0.89 \pm 0.07</i>	1.35 \pm 0.39
	0.55 \pm 0.01	0.19 \pm 0.27	<i>0.65 \pm 0.03</i>	0.05 \pm 0.46	0.59 \pm 0.06	0.26 \pm 0.17	0.66 \pm 0.01	0.15 \pm 0.33	0.64 \pm 0.05	0.15 \pm 0.29

from scratch using the observed FLUXNET-CH₄ dataset, which is the same as the results reported in Table 2. The remaining columns correspond to various transfer learning strategies. A key observation is that transfer learning generally improves model performance compared to training from scratch, particularly in temporal extrapolation tasks. Most models benefit from transfer learning, showing reduced error and improved predictive accuracy. This suggests that simulated data can help capture fundamental methane flux dynamics, thereby improving model performance on limited observation data. Notably, temporal extrapolation results remain relatively stable across different model initializations, leading to consistently small standard deviations. In contrast, spatial extrapolation exhibits substantially higher variability across cross-validation folds. This increased variance primarily reflects the strong spatial heterogeneity of methane fluxes: different train-test region splits induce markedly different data distributions, resulting in large performance fluctuations across folds. Overall, these results indicate that while temporal dependencies can be learned in a relatively consistent manner, spatial generalization remains considerably more challenging due to pronounced geographical heterogeneity.

Comparing the performance of each model in Table 3, we observe that LSTM performs well even when trained from scratch, demonstrating its effectiveness in handling limited data. LSTM further improves when applying any of the four transfer learning approaches. In contrast, EA-LSTM initially performs worse than LSTM when trained from scratch but significantly improves with transfer learning, especially using data transfer methods. A similar pattern is observed in Transformer. Due to its large number of parameters, it is difficult to train effectively with a limited amount of data, resulting in very poor performance when trained from scratch. In contrast, its performance improves significantly with transfer learning from the simulated data, becoming comparable with LSTM-based models. Pyraformer outperforms other Transformer-based models and demonstrates strong performance even when trained from scratch. Such data efficiency is likely attributed to the reduced complexity introduced by the pyramid attention mechanism, which enhances computational efficiency compared with traditional

Transformers. Additionally, the hierarchical pyramid structure progressively aggregates information at multiple time scales, enabling Pyraformer to effectively capture long-term dependencies. TCN and iTransformer exhibit the worst performance among all models. Both models fail to adapt well to complex temporal patterns, resulting in significantly lower predictive performance.

Among the transfer learning approaches, fine-tuning achieves the most consistent improvements across both temporal and spatial extrapolation tasks, demonstrating the effectiveness of leveraging simulated data to enhance model generalization. The residual and adversarial training methods show varying degrees of effectiveness, with some models benefiting more than others. These methods appear to improve generalization in certain cases, but their performance is less stable compared to standard fine-tuning. The re-weighting approach, which assigns importance to different training samples, exhibits mixed results, with some models improving while others show a slight degradation in performance, particularly in spatial extrapolation. This indicates that while re-weighting strategies may be beneficial in certain scenarios, they require careful selection of similarity measures to ensure performance improvement. Overall, transfer learning proves to be a valuable strategy for methane flux prediction, particularly when models are pre-trained using simulated data before fine-tuning on real observations. These results highlight the importance of combining data-driven approaches and scientific knowledge from physics-based models.

Qualitative Analysis. To further investigate the predictive behavior of our framework, we visualize representative examples of the fine-tuned LSTM model’s predictions for both temporal and spatial extrapolation tasks (Figure 5). In the temporal extrapolation task (predicting held-out years at seen sites), the model effectively captures the seasonal phenology and general flux magnitude. However, in the spatial extrapolation task (predicting held-out sites), the performance drops, reflecting the intrinsic difficulty of generalising to unseen geographical contexts. This performance gap is primarily driven by the extreme spatial heterogeneity of the FLUXNET-CH₄ dataset, where methane emission patterns vary significantly across different wetland types and microclimates.

Table 4: Relative predictive uncertainty ($std/mean$ ratio) across different models and transfer learning schemes, where lower values indicate higher model confidence. *None: no transfer; FT: fine-tuning; Res: residual adaptation; Adv: adversarial; RW: re-weighting.*

Model	None	FT	Res	Adv	RW	Avg
LSTM	0.156	0.155	0.221	0.120	0.186	0.168
EA-LSTM	0.199	0.189	0.250	0.164	0.191	0.199
TCN	0.301	0.333	0.368	0.330	0.315	0.329
Transformer	0.220	0.378	0.388	0.250	0.290	0.305
iTransformer	0.302	0.243	0.336	0.147	0.128	0.231
Pyraformer	0.148	0.148	0.133	0.191	0.218	0.168
Average	0.221	0.241	0.283	0.200	0.221	0.233

Uncertainty and reliability analysis. While our main experimental results report the ensemble-based uncertainty (mean \pm std) derived from independently trained models, it is equally critical to quantify the intrinsic predictive confidence of each individual model. To this end, we further employ Monte Carlo Dropout ($p = 0.2$ with 100 stochastic forward passes) at inference time to compute the relative predictive uncertainty ($std/mean$ ratio). This metric, reported in Table 4, reflects the model’s internal stability when facing data perturbations.

The quantitative results reveal significant insights into the reliability of transfer learning. On the strategy level, adversarial learning consistently achieves the lowest average uncertainty across all architectures, suggesting that explicitly aligning the feature distributions of simulations and observations effectively filters out simulation biases, leading to more confident predictions. Regarding model architectures, both Pyraformer and LSTM emerge as the most robust baselines. While LSTM benefits from its architectural simplicity, Pyraformer’s robustness highlights the efficacy of its hierarchical pyramid attention in regularizing long-range temporal dependencies. Notably, we observe a ‘stability-accuracy gap’ in models like iTransformer, which can achieve low specific uncertainty (0.128 under Re-weighting) but suffer from poor predictive accuracy (Table 3). This indicates that such models may converge to consistently biased minima rather than capturing the high-frequency flux dynamics, underscoring that low uncertainty must be paired with high accuracy to serve as a valid benchmark.

5.5 Sparsity test in transfer learning

To mimic real-world challenges in data collection, we also conduct a series of sparsity tests in the temporal extrapolation task. We used 50%, 20%, 10%, and 5% of the original FLUXNET-CH₄ training data to train both LSTM and Transformer models across three learning scenarios: (1) training from scratch, (2) data transfer using DANN, and (3) parameter transfer via fine-tuning. This approach demonstrates that these models can still exhibit promising generalizability even when the training data is severely limited.

According to the results shown in Figure 6, we have some observations: (1) Both LSTM and Transformer degrade when less data is available, especially at the 5% level; (2) both transfer methods (data transfer and parameter transfer) outperform training from scratch, with the most significant gains at 10% and 5%; (3) parameter transfer via fine-tuning serves as a strong middle ground, bridging the

gap between scratch and data approaches in moderate to low data scenarios; (4) the data transfer approach (DANN) used in LSTM yields the lowest error across all training percentages, even at 5%; (5) while the Transformer does well with sufficient data, it is more sensitive to data sparsity than the LSTM, though both architectures benefit greatly from transfer strategies rather than training from scratch. Overall, these findings confirm that both transfer learning approaches (i.e., DANN and transferring pre-trained parameters) effectively reduce the impact of limited observation data in training. This offers new insights into the use of advanced ML models in real-world situations where large observation data are unavailable.

6 Conclusion and Future Work

This paper introduces X-MethaneWet as the first integrative wetland CH₄ dataset combining both TEM-MDM-based simulations and true observations of methane emissions. The dataset is collected at a daily time interval across the entire globe while maintaining distinct scales between the simulated and observed data. We create a standardized evaluation framework and also conduct extensive experiments using multiple types of ML models. Our results demonstrate the promise of certain ML models in generalizing to unobserved spatial regions and future time periods. The transfer learning experiment also underscores the potential of a hybrid learning paradigm that integrates physical simulations with data-driven modeling of truly observed methane emissions.

We would like to acknowledge the limitations of this study. Firstly, the global CO₂ and CH₄ concentration and NPP used in this study are at annual or monthly temporal resolution due to the data availability. Also, soil properties and vegetation are assumed static because they are temporally stable and less likely to change over decades unless there is significant land disturbance. In the future, augmenting these variables to a higher temporal resolution could further improve the model’s accuracy. Secondly, this study makes use of existing wetland eddy covariance sites, although observational coverage is sparse in tropical regions. We advocate for the establishment of new observation sites in tropical regions, which would significantly improve CH₄ emission estimates [73].

The X-MethaneWet dataset could serve as an important resource to catalyze the exploration of new data mining and machine learning algorithms for predicting global methane emissions. This can greatly facilitate the development of tools for decision making in methane mitigation. Future work includes integrating other methane data sources, such as top-down atmospheric inversions [65], and exploring advanced knowledge-guided learning methods for combining physics-based models and ML algorithms.

Acknowledgments

This work was supported by the National Science Foundation (NSF) grants 2239175, 2316305, 2147195, 2425844, 2425845, 2430978, 2126474, 2530609, 2530610, and 2203581, and 2153040; USGS awards G21AC10564 and G22AC00266; NASA grants 80NSSC24K1061 and 80NSSC25K0013; Department of Energy (DOE) grant DE-SC0024360; USDA and NSF funded AI institute AI-LEAF: 2023-67021-39829; and NSF NCAR’s Derecho HPC system. This research was also supported in part by the University of Pittsburgh Center for Research Computing.

References

- [1] Hana Ajakan, Pascal Germain, Hugo Larochelle, François Laviolette, and Mario Marchand. 2014. Domain-adversarial neural networks. *arXiv preprint arXiv:1412.4446* (2014).
- [2] Brian Bergamaschi and Lisamarie Windham-Myers. 2018. FLUXNET-CH4 US-Srr Suisun marsh-Rush Ranch. doi:10.18140/FLX/1669694
- [3] P. Bergamaschi, S. Houweling, A. Segers, M. Krol, C. Frankenberg, R. A. Scheepmaker, E. Dlugokencky, S. C. Wofsy, E. A. Kort, C. Sweeney, T. Schuck, C. Brenninkmeijer, H. Chen, V. Beck, and C. Gerbig. 2013. Atmospheric CH₄ in the first decade of the 21st century: Inverse modeling analysis using SCIAMACHY satellite retrievals and NOAA surface measurements. *Journal of Geophysical Research: Atmospheres* 118, 13 (2013), 7350–7369. doi:10.1002/jgrd.50480
- [4] Gil Bohrer. 2016. FLUXNET-CH4 US-ORv Olentangy River Wetland Research Park. doi:10.18140/FLX/1669689
- [5] Gil Bohrer and Janice Kerns. 2018. FLUXNET-CH4 US-OWC Old Woman Creek. doi:10.18140/FLX/1669690
- [6] AJ Carter and RJ Scholes. 1999. Generating a global database of soil properties. *Environmentek CSIR* 10 (1999).
- [7] Jiquan Chen and Housen Chu. 2016. FLUXNET-CH4 US-WPT Winous Point North Marsh. doi:10.17190/AMF/1246155
- [8] Shuo Chen, Licheng Liu, Ma Yuchi, Qianlai Zhuang, and N. J. Shurpali. 2024. Quantifying global wetland methane emissions with in situ methane flux data and machine learning approaches. *Earth's Future* 12 (2024). doi:10.1029/2023EF004330
- [9] Dick P Dee, SM Uppala, Adrian J Simmons, Paul Berrisford, Paul Poli, Shinya Kobayashi, U Andrae, MA Balmaseda, G Balsamo, et al. 2011. The ERA-Interim reanalysis: Configuration and performance of the data assimilation system. *Quarterly Journal of the royal meteorological society* 137, 656 (2011), 553–597.
- [10] Kyle B Delwiche, Sara Helen Knox, Avni Malhotra, Etienne Fluet-Chouinard, Gavin McNicol, Sarah Feron, Zutao Ouyang, Dario Papale, Carlo Trotta, Eleonora Canfora, et al. 2021. FLUXNET-CH4: A global, multi-ecosystem dataset and analysis of methane seasonality from freshwater wetlands. *Earth System Science Data Discussions* 2021 (2021), 1–111.
- [11] Ankur Desai. 2016. FLUXNET-CH4 US-Los Lost Creek. doi:10.18140/FLX/1669682
- [12] Eugenie Euskirchen and Colin Edgar. 2020. FLUXNET-CH4 US-BZF Bonanza Creek Rich Fen, United States. doi:10.18140/FLX/1669669
- [13] Zhihan Gao, Xingjian Shi, Hao Wang, Yi Zhu, Yuyang Bernie Wang, Mu Li, and Dit-Yan Yeung. 2022. Earthformer: Exploring space-time transformers for earth system forecasting. *Advances in Neural Information Processing Systems* 35 (2022), 25390–25403.
- [14] Mathias Goeckede. 2020. FLUXNET-CH4 RU-Che Cherski, Russian Federation. doi:10.18140/FLX/1669655
- [15] Jaclyn A. Hatala, Matteo Detto, and Dennis D. Baldocchi. 2012. Gross ecosystem photosynthesis causes a diurnal pattern in methane emission from rice. *Geophysical Research Letters* 39, 6 (2012). doi:10.1029/2012GL051303
- [16] Carole Helfter. 2020. FLUXNET-CH4 BW-Gum Guma, Botswana. doi:10.18140/FLX/1669370
- [17] Charless Ross Hinkle. 2016. FLUXNET-CH4 US-DPW Disney Wilderness Preserve Wetland. doi:10.18140/FLX/1669672
- [18] S Hochreiter. 1997. Long Short-term Memory. *Neural Computation MIT-Press* (1997).
- [19] Sepp Hochreiter and Jürgen Schmidhuber. 1997. Long Short-Term Memory. *Neural Computation* 9, 8 (1997), 1735–1780. doi:10.1162/neco.1997.9.8.1735
- [20] Jeremy Irvin, Sharon Zhou, Gavin McNicol, Fred Lu, Vincent Liu, Etienne Fluet-Chouinard, Zutao Ouyang, Sara Helen Knox, Antje Lucas-Moffat, Carlo Trotta, Dario Papale, Domenico Vitale, Ivan Mammarella, Pavel Alekseychik, Mika Aurela, Anand Avati, Dennis Baldocchi, Sheel Bansal, Gil Bohrer, David I Campbell, Jiquan Chen, Housen Chu, Higo J Dalmagro, Kyle B Delwiche, Ankur R Desai, Eugenie Euskirchen, et al. 2021. Gap-filling eddy covariance methane fluxes: Comparison of machine learning model predictions and uncertainties at FLUXNET-CH4 wetlands. *Agricultural and Forest Meteorology* 308-309 (Oct. 2021), 108528. doi:10.1016/j.agrformet.2021.108528
- [21] R. B. Jackson, M. Saunio, A. Martinez, J. G. Canadell, X. Yu, M. Li, B. Poulter, P. A. Raymond, P. Regnier, P. Ciais, S. J. Davis, and P. K. Patra. 2024. Human activities now fuel two-thirds of global methane emissions. *Environmental Research Letters* 19, 10 (Sept. 2024), 101002. doi:10.1088/1748-9326/ad6463
- [22] A Jacotot, S Gogo, and F Laggoun-Défarge. 2020. FLUXNET-CH4 FR-LGt La Gnette, France. doi:10.18140/FLX/1669641
- [23] Xiaowei Jia, Jared Willard, Anuj Karpatne, Jordan S Read, Jacob A Zwart, Michael Steinbach, and Vipin Kumar. 2021. Physics-guided machine learning for scientific discovery: An application in simulating lake temperature profiles. *ACM/IMS Transactions on Data Science* 2, 3 (2021), 1–26.
- [24] Anuj Karpatne, Xiaowei Jia, and Vipin Kumar. 2024. Knowledge-guided machine learning: Current trends and future prospects. *arXiv preprint arXiv:2403.15989* (2024).
- [25] Anuj Karpatne, Ramakrishnan Kannan, and Vipin Kumar. 2022. *Knowledge guided machine learning: Accelerating discovery using scientific knowledge and data*. CRC Press.
- [26] Yeonuk Kim, Mark S. Johnson, Sara H. Knox, T. Andrew Black, Higo J. Dalmagro, Minseok Kang, Joon Kim, and Dennis Baldocchi. 2020. Gap-filling approaches for eddy covariance methane fluxes: A comparison of three machine learning algorithms and a traditional method with principal component analysis. *Global Change Biology* 26, 3 (2020), 1499–1518. doi:10.1111/gcb.14845
- [27] Sara H. Knox, Robert B. Jackson, Benjamin Poulter, Gavin McNicol, Etienne Fluet-Chouinard, Zhen Zhang, Gustaf Hugelius, Philippe Bousquet, Josep G. Canadell, Marielle Saunio, Dario Papale, Housen Chu, Trevor F. Keenan, Dennis Baldocchi, Margaret S. Torn, Ivan Mammarella, Carlo Trotta, Mika Aurela, Gil Bohrer, et al. 2019. FLUXNET-CH4 Synthesis Activity: Objectives, Observations, and Future Directions. (Dec. 2019). doi:10.1175/BAMS-D-18-0268.1
- [28] Franziska Koebisch and Gerald Jurasinski. 2020. FLUXNET-CH4 DE-Hte Huetelmoor, Germany. doi:10.18140/FLX/1669634
- [29] Frederik Kratzert, Daniel Klotz, Guy Shalev, Günter Klambauer, Sepp Hochreiter, and Grey Nearing. 2019. Benchmarking a catchment-aware long short-term memory network (LSTM) for large-scale hydrological modeling. *Hydrology and Earth System Sciences Discussions* (2019), 1–32.
- [30] Frederik Kratzert, Daniel Klotz, Guy Shalev, Günter Klambauer, Sepp Hochreiter, and Grey Nearing. 2019. Towards learning universal, regional, and local hydrological behaviors via machine learning applied to large-sample datasets. *Hydrology and Earth System Sciences* 23, 12 (2019), 5089–5110.
- [31] Ken Krauss. 2019. FLUXNET-CH4 US-LA1 Pointe-aux-Chenes Brackish Marsh. doi:10.18140/FLX/1669680
- [32] Ken Krauss. 2019. FLUXNET-CH4 US-LA2 Salvador WMA Freshwater Marsh. doi:10.18140/FLX/1669681
- [33] Colin Lea, Michael D Flynn, Rene Vidal, Austin Reiter, and Gregory D Hager. 2017. Temporal convolutional networks for action segmentation and detection. In *proceedings of the IEEE Conference on Computer Vision and Pattern Recognition*. 156–165.
- [34] Youru Li, Zhenfeng Zhu, Deqiang Kong, Hua Han, and Yao Zhao. 2019. EA-LSTM: Evolutionary attention-based LSTM for time series prediction. *Knowledge-Based Systems* 181 (2019), 104785.
- [35] Jiangtao Liu, Yuchen Bian, Kathryn Lawson, and Chaopeng Shen. 2024. Probing the limit of hydrologic predictability with the Transformer network. *Journal of Hydrology* 637 (2024), 131389.
- [36] Licheng Liu, Wang Zhou, Kaiyu Guan, Bin Peng, Shaoming Xu, Jinyun Tang, Qing Zhu, Jessica Till, Xiaowei Jia, Chongya Jiang, Sheng Wang, Ziqi Qin, Hui Kong, Robert Grant, Symon Mezbahuddin, Vipin Kumar, and Zhenong Jin. 2024. Knowledge-guided machine learning can improve carbon cycle quantification in agroecosystems. *Nature Communications* 15, 1 (Jan. 2024), 357. doi:10.1038/s41467-023-43860-5
- [37] Shizhan Liu, Hang Yu, Cong Liao, Jianguo Li, Weiyao Lin, Alex X Liu, and Schahram Dustdar. 2022. Pyraformer: Low-complexity pyramidal attention for long-range time series modeling and forecasting. In # *PLACEHOLDER_PARENT_METADATA_VALUE#*.
- [38] Yujie Liu, Hongbin Dong, Xingmei Wang, and Shuang Han. 2019. Time series prediction based on temporal convolutional network. In *2019 IEEE/ACIS 18th International conference on computer and information science (ICIS)*. IEEE, 300–305.
- [39] Yong Liu, Tengge Hu, Haoran Zhang, Haixu Wu, Shiyu Wang, Lintao Ma, and Mingsheng Long. 2023. itransformer: Inverted transformers are effective for time series forecasting. *arXiv preprint arXiv:2310.06625* (2023).
- [40] Annalea Lohila, Mika Aurela, Juha-Pekka Tuovinen, Tuomas Laurila, Juha Hatakka, Juuso Rainne, and Timo Mäkelä. 2020. FLUXNET-CH4 FI-Lom Lompolojankka, Finland. doi:10.18140/FLX/1669638
- [41] Jaclyn Hatala Matthes, Cove Sturtevant, Patty Oikawa, Samuel D Chamberlain, Daphne Szutu, Ariane Arias-Ortiz, Joseph Verfaillie, and Dennis Baldocchi. 2016. FLUXNET-CH4 US-Myb Mayberry Wetland. doi:10.18140/FLX/1669685
- [42] Elaine Matthews and Inez Fung. 1987. Methane emission from natural wetlands: Global distribution, area, and environmental characteristics of sources. *Global biogeochemical cycles* 1, 1 (1987), 61–86.
- [43] John A Matthews. 1999. ON RECENTLY-DEGLACIATED SUBSTRATES. *Ecosystems of disturbed ground* 16 (1999), 17.
- [44] Gavin McNicol, Etienne Fluet-Chouinard, Zutao Ouyang, Sara Knox, Zhen Zhang, Tuula Aalto, Sheel Bansal, Kuang-Yu Chang, Min Chen, Kyle Delwiche, Sarah Feron, Mathias Goeckede, Jinxun Liu, Avni Malhotra, Joe R. Melton, William Riley, Rodrigo Vargas, Kunxiao Jia, Qing Ying, Qing Zhu, et al. 2023. Upscaling Wetland Methane Emissions From the FLUXNET-CH4 Eddy Covariance Network (UpCH4 v1.0): Model Development, Network Assessment, and Budget Comparison. *AGU Advances* 4, 5 (2023), e2023AV000956. doi:10.1029/2023AV000956
- [45] Jerry M Melillo, A David McGuire, David W Kicklighter, Berrien Moore, Charles J Vorosmarty, and Annette L Schloss. 1993. Global climate change and terrestrial net primary production. *Nature* 363, 6426 (1993), 234–240.
- [46] Freddy Nachtergaele, Harrij van Velthuisen, Luc Verelst, Niels Batjes, Koos Dijkshoorn, Vincent van Engelen, Guenther Fischer, Arwyn Jones, Luca Montanarella, Monica Petri, et al. 2010. Harmonized world soil database. In *Proceedings of the 19th world congress of soil science, soil solutions for a changing world, Brisbane, Australia*, Vol. 2010. International Union of Soil Sciences, 34–37.

- [47] Scott C Neubauer and J Patrick Meconigal. 2015. Moving beyond global warming potentials to quantify the climatic role of ecosystems. *Ecosystems* 18 (2015), 1000–1013.
- [48] Asko Noormets, John King, Bhaskar Mitra, Guofang Miao, Maricar Aguilos, Kevan Minick, Prajaya Prajapati, Jean-Christophe Domec, Jonathan Furst, and Maxwell Wightman. 2020. FLUXNET-CH4 US-NC4 NC_AlligatorRiver. doi:10.18140/FLX/1669686
- [49] Gilberto Pastorello, Carlo Trotta, Eleonora Canfora, Housen Chu, Danielle Christianson, You-Wei Cheah, Cristina Poindexter, Jiquan Chen, Abdelrahman El-bashandy, Marty Humphrey, et al. 2020. The FLUXNET2015 dataset and the ONEFlux processing pipeline for eddy covariance data. *Scientific data* 7, 1 (2020), 225.
- [50] Charlotte Pelletier, Geoffrey I Webb, and François Petitjean. 2019. Temporal convolutional neural network for the classification of satellite image time series. *Remote Sensing* 11, 5 (2019), 523.
- [51] Olli Peltola, Timo Vesala, Yao Gao, Olle Räty, Pavel Alekseychik, Mika Aurela, Bogdan Chojnicki, Ankur R Desai, Albertus J Dolman, Eugenie S Euskirchen, et al. 2019. Monthly gridded data product of northern wetland methane emissions based on upscaling eddy covariance observations. *Earth System Science Data* 11, 3 (2019), 1263–1289.
- [52] Stephan Rasp and Nils Thuerey. 2021. Data-driven medium-range weather prediction with a resnet pretrained on climate simulations: A new model for weatherbench. *Journal of Advances in Modeling Earth Systems* 13, 2 (2021).
- [53] Jordan S Read, Xiaowei Jia, Jared Willard, Alison P Appling, Jacob A Zwart, Samantha K Oliver, Anuj Karpatne, Gretchen JA Hansen, Paul C Hanson, William Watkins, et al. 2019. Process-guided deep learning predictions of lake water temperature. *Water Resources Research* 55, 11 (2019), 9173–9190.
- [54] Torsten Sachs, Christian Wille, Eric Larmanou, and Daniela Franz. 2020. FLUXNET-CH4 DE-Zrk Zarnekow, Germany. doi:10.18140/FLX/1669636
- [55] Marielle Sauniois, Adrien Martinez, Benjamin Poulter, Zhen Zhang, Peter Raymond, Pierre Regnier, Joseph G. Canadell, Robert B. Jackson, Prabir K. Patra, Philippe Bousquet, Philippe Ciais, Edward J. Dlugokencky, Xin Lan, George H. Allen, David Bastviken, David J. Beerling, Dmitry A. Belikov, et al. 2024. Global Methane Budget 2000–2020. *Earth System Science Data Discussions* (June 2024), 1–147. doi:10.5194/essd-2024-115
- [56] Karina Schafer. 2020. *FLUXNET-CH4 US-MRM Marsh Resource Meadowlands Mitigation Bank*. Technical Report. FluxNet.
- [57] Hans Peter Schmid and Janina Klatt. 2020. FLUXNET-CH4 DE-SIN Schechenfilz Nord, Germany. doi:10.18140/FLX/1669635
- [58] Oliver Sonnentag and William L Quinton. 2019. FLUXNET-CH4 AmeriFlux CA-SCB Scotty Creek Bog. doi:10.18140/FLX/1669613
- [59] Thomas F. Stocker. 2013. *Climate change 2013: the physical science basis: summary for policymakers, a report of Working Group I of the IPCC, technical summary, a report accepted by Working Group I of the IPCC but not approved in detail and frequently asked questions: part of the Working Group I contribution to the fifth assessment report of the Intergovernmental Panel on Climate Change*. Intergovernmental Panel on Climate Change, New York.
- [60] Alexander Y Sun, Peishi Jiang, Maruti K Mudunuru, and Xingyuan Chen. 2021. Explore spatio-temporal learning of large sample hydrology using graph neural networks. *Water Resources Research* 57, 12 (2021), e2021WR030394.
- [61] Hanqin Tian, Guangsheng Chen, Chaoqun Lu, Xiaofeng Xu, Wei Ren, Bowen Zhang, Kamaljit Banger, Bo Tao, Shufen Pan, Mingliang Liu, Chi Zhang, Lori Bruhwiler, and Steven Wofsy. 2015. Global methane and nitrous oxide emissions from terrestrial ecosystems due to multiple environmental changes. *Ecosystem Health and Sustainability* 1, 1 (March 2015), 1–20. doi:10.1890/EHS14-0015.1
- [62] Simon N Topp, Janet Barclay, Jeremy Diaz, Alexander Y Sun, Xiaowei Jia, Dan Lu, Jeffrey M Sadler, and Alison P Appling. 2023. Stream temperature prediction in a shifting environment: Explaining the influence of deep learning architecture. *Water Resources Research* 59, 4 (2023), e2022WR033880.
- [63] Thierry Toutin. 2002. Three-dimensional topographic mapping with ASTER stereo data in rugged topography. *IEEE Transactions on geoscience and remote sensing* 40, 10 (2002), 2241–2247.
- [64] Masahito Ueyama, Takashi Hirano, and Yasuhiro Kominami. 2020. FLUXNET-CH4 JP-BBY Bibai bog, Japan. doi:10.18140/FLX/1669646
- [65] Samuel Upton, Markus Reichstein, Fabian Gans, Wouter Peters, Basil Kraft, and Ana Bastos. 2024. Constraining biospheric carbon dioxide fluxes by combined top-down and bottom-up approaches. *Atmospheric Chemistry and Physics* 24, 4 (2024), 2555–2582.
- [66] Ashish Vaswani, Noam Shazeer, Niki Parmar, Jakob Uszkoreit, Llion Jones, Aidan N Gomez, Lukasz Kaiser, and Illia Polosukhin. 2017. Attention is all you need. *Advances in neural information processing systems* 30 (2017).
- [67] Timo Vesala, Eeva-Stiina Tuittila, Ivan Mammarella, and Pavel Alekseychik. 2020. FLUXNET-CH4 FI-Si2 Siikaneva-2 Bog, Finland. doi:10.18140/FLX/1669639
- [68] Jared Willard, Xiaowei Jia, Shaoming Xu, Michael Steinbach, and Vipin Kumar. 2022. Integrating scientific knowledge with machine learning for engineering and environmental systems. *Comput. Surveys* 55, 4 (2022), 1–37.
- [69] Runlong Yu, Chonghao Qiu, Robert Ladwig, Paul C Hanson, Yiqun Xie, Yanhua Li, and Xiaowei Jia. 2024. Adaptive Process-Guided Learning: An Application in Predicting Lake DO Concentrations. *arXiv preprint arXiv:2411.12973* (2024).
- [70] Kunxiaoia Yuan, Qing Zhu, Fa Li, William J. Riley, Margaret Torn, Housen Chu, Gavin McNicol, Min Chen, Sara Knox, Kyle Delwiche, Huayi Wu, Dennis Baldocchi, Hongxu Ma, Ankur R. Desai, Jiquan Chen, Torsten Sachs, Masahito Ueyama, Oliver Sonnentag, Manuel Helbig, Eeva-Stiina Tuittila, Gerald Jurasinski, et al. 2022. Causality guided machine learning model on wetland CH4 emissions across global wetlands. *Agricultural and Forest Meteorology* 324 (Sept. 2022), 109115. doi:10.1016/j.agrformet.2022.109115
- [71] Zhen Zhang, Etienne Fluet-Chouinard, Katherine Jensen, Kyle McDonald, Gustaf Hugelius, Thomas Gumbrecht, Mark Carroll, Catherine Prigent, Annett Bartsch, and Benjamin Poulter. 2021. Development of the global dataset of wetland area and dynamics for methane modeling (WAD2M). *Earth System Science Data* 13, 5 (2021), 2001–2023.
- [72] Zhen Zhang, Niklaus E. Zimmermann, Andrea Stenke, Xin Li, Elke L. Hodson, Gaofeng Zhu, Chunlin Huang, and Benjamin Poulter. 2017. Emerging role of wetland methane emissions in driving 21st century climate change. *Proceedings of the National Academy of Sciences* 114, 36 (Sept. 2017), 9647–9652. doi:10.1073/pnas.1618765114
- [73] Qing Zhu, Kunxiaoia Yuan, Fa Li, William J Riley, Alison Hoyt, Robert Jackson, Gavin McNicol, Min Chen, Sara H Knox, Otto Briner, et al. 2024. Critical needs to close monitoring gaps in pan-tropical wetland CH4 emissions. *Environmental Research Letters* 19, 11 (2024), 114046.
- [74] Q Zhuang, AD McGuire, JM Melillo, JS Klein, RJ Dargaville, DW Kicklighter, RB Myneni, J Dong, VE Romanovsky, J Harden, et al. 2003. Carbon cycling in extratropical terrestrial ecosystems of the Northern Hemisphere during the 20th Century: A modeling analysis of the influences of soil thermal dynamics, Tellus, 55 B, 751–776, 2003. *REPORT SERIES of the MIT Joint Program on the Science and Policy of Global Change* (2003).
- [75] Q. Zhuang, J. M. Melillo, D. W. Kicklighter, R. G. Prinn, A. D. McGuire, P. A. Steudler, B. S. Felzer, and S. Hu. 2004. Methane fluxes between terrestrial ecosystems and the atmosphere at northern high latitudes during the past century: A retrospective analysis with a process-based biogeochemistry model. *Global Biogeochemical Cycles* 18, 3 (2004). doi:10.1029/2004GB002239
- [76] Donatella Zona and Walter Oechel. 2016. FLUXNET-CH4 US-Ivo Ivtok. doi:10.18140/FLX/1669679
- [77] Donatella Zona and Walter C Oechel. 2020. FLUXNET-CH4 US-Atq Atqasuk, United States. doi:10.18140/FLX/1669663
- [78] Donatella Zona and Walter C Oechel. 2020. FLUXNET-CH4 US-Beo Barrow Environmental Observatory (BEO) tower, United States. doi:10.18140/FLX/1669664
- [79] Donatella Zona and Walter C Oechel. 2020. FLUXNET-CH4 US-Bes Barrow-Bes (Biocomplexity Experiment South tower), United States. doi:10.18140/FLX/1669665

A Detailed descriptions of TEM-MDM features

To better understand the characteristics of the TEM-MDM dataset, we provide a detailed breakdown of its features:

Variable (Symbol, Unit)	Min	Max	Mean / Median
Precipitation (PREC, mm/day)	0	534	2
Air temperature (TAIR, °C)	-71	47	9
Solar radiance (SOLR, W/m ⁻²)	0	452	175
Vapor pressure (VAPR, hPa)	0	46	10
Topsoil bulk density (kg/dm ³)	0	2	1
Soil texture fraction (clfaotxt, %)	25	80	49
Soil pH (pH2o)	0	9	6
Elevation (clelev, m)	-51	6130	671 (median)
Net primary productivity (NPP, gC m ⁻² month ⁻¹)	-387	315	25

The spatial distribution of categorical vegetation type, plant function type, wetland type, and climate type are shown in Figure 7.

B Detailed descriptions of 30 FLUXNET-CH4 sites

Figure 8 presents the geographic locations and wetland types of 30 FLUXNET-CH4 sites. From the figure, we observe that FLUXNET-CH4 sites span multiple continents and are unevenly distributed worldwide, with some locations being geographically isolated. Additionally, the distribution of wetland types varies across sites, indicating regional deviations in wetland ecosystems.

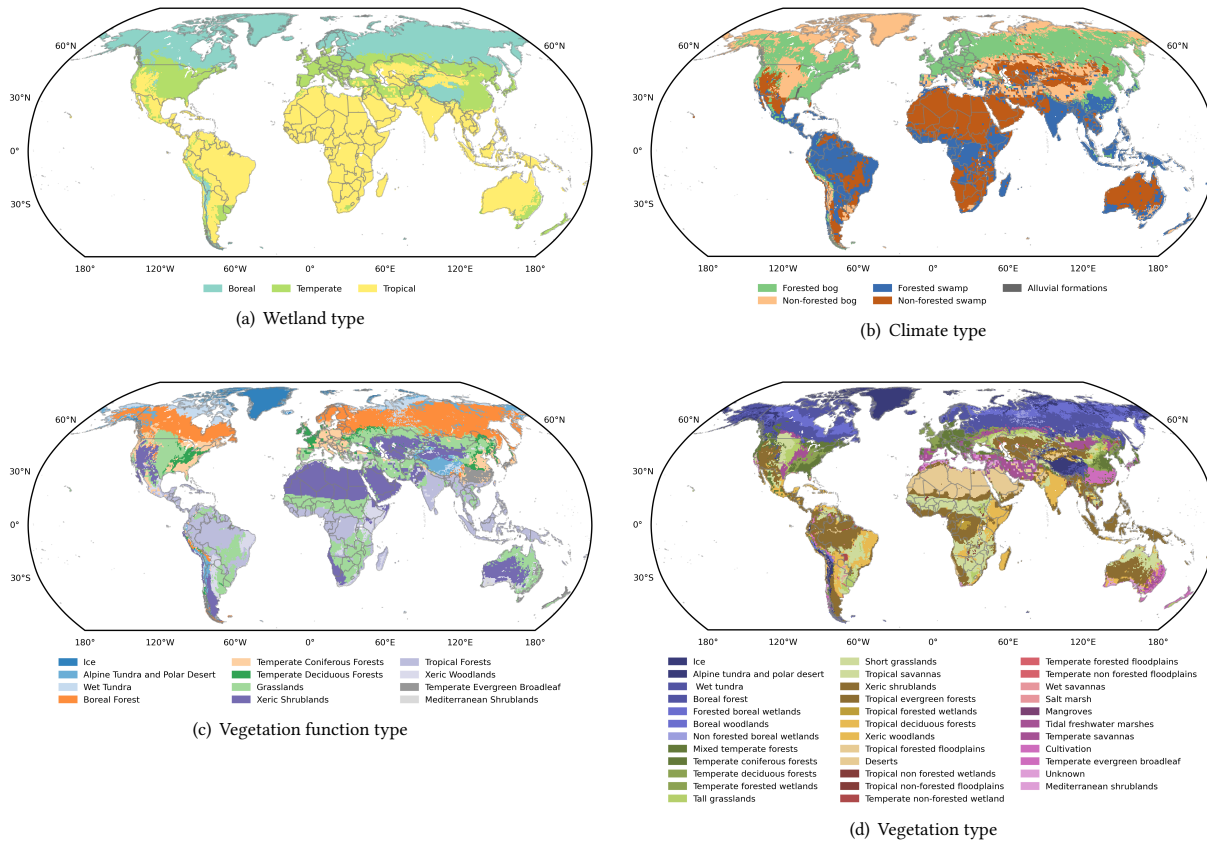


Figure 7: Spatial distribution of wetland type, climate type, vegetation function type and vegetation type.

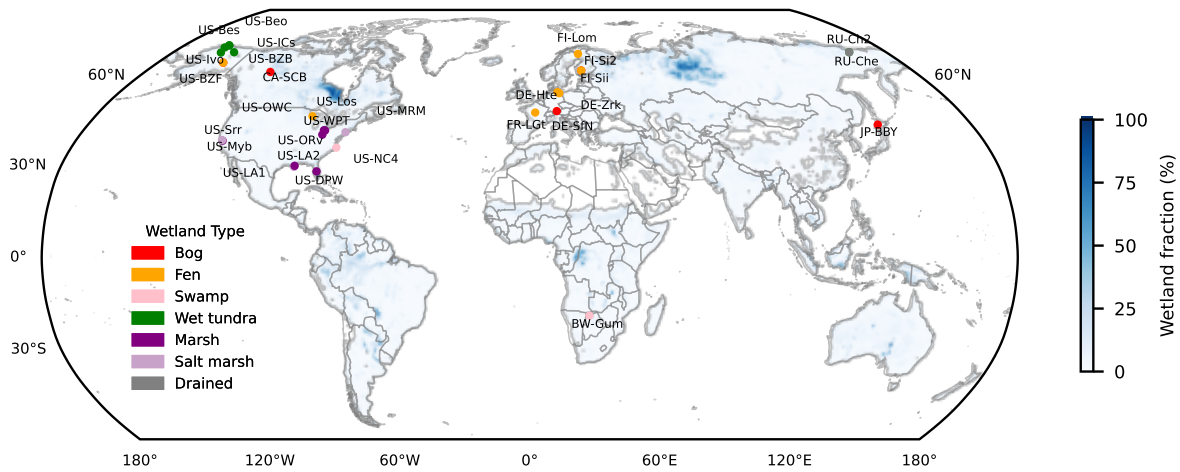


Figure 8: Location and wetland type of 30 FLUXNET-CH₄ sites. Symbol colors represent the wetland type. The wetland fraction was derived from the WAD2M wetland distribution map [71].